Article

# Arginine-presenting peptide hydrogels decorated with hydroxyapatite as biomimetic scaffolds for bone regeneration

Moumita Ghosh, Michal Halperin-Sternfeld, Irena Grigoriants, Jaehun Lee, Ki Tae Nam, and Lihi Adler-Abramovich

*Biomacromolecules*, **Just Accepted Manuscript** • DOI: 10.1021/acs.biomac.7b00876 • Publication Date (Web): 21 Aug 2017



## Just Accepted



Biomacromolecules is published by the American Chemical Society. 1155 Sixteenth Street N.W., Washington, DC 20036

# Arginine-presenting peptide hydrogels decorated with hydroxyapatite as biomimetic scaffolds for bone regeneration

*Moumita Ghosh*[‡1], *Michal Halperin-Sternfeld*[‡1], *Irena Grigoriants*[1], *Jaehun Lee*[2], *Ki Tae Nam*[2] *and Lihi Adler-Abramovich*[1]*

[1]Department of Oral Biology, The Goldschleger School of Dental Medicine, Sackler Faculty of Medicine, Tel-Aviv University 69978, ISRAEL

[2]Department of Materials Science and Engineering, Seoul National University, Seoul, 151-744, Korea

[‡]These authors contributed equally to this work

*Correspondence to: LihiA@tauex.tau.ac.il

Keywords: Low molecular weight hydrogels; Bone regeneration; Hydroxyapatite; Self-assembly; peptides

## Abstract

Hydrogels are promising candidates for biomimetic scaffolds of the extracellular matrix in tissue engineering applications. However, their use in bone tissue-engineering is limited due to their low mechanical properties. In this study, we designed and synthesized multi-component peptide-based hydrogels composed of Fluorenyl-9-methoxycarbonyl diphenylalanine (FmocFF), that contributed to the rigidity and stability of the hydrogel, and Fmoc-arginine (FmocR), which mediated high affinity to hydroxyapatite (HAP) due to the arginine moiety. The new hydrogels composed of nanometric fibrils networks were decorated with HAP and demonstrated high mechanical strength with a storage modulus of up to 29 kPa. In addition, the hydrogels supported cell adhesion and *in vitro* cell viability. These properties suggest using these multi-component organic-inorganic hydrogels as functional biomaterials for improved bone regeneration.

## Introduction

Natural bone is an organic-inorganic nanocomposite, well-known for its remarkable mechanical performance, including high strength and fracture toughness.[1, 2] However, bone may become diseased or damaged, resulting in irregularly shaped defects, which require challenging cranio-facial and orthopedic reconstructive surgeries.[1, 3, 4] Autogenous bone has been considered the gold standard for bone grafting due to its osteoconductive, osteoinductive and osteogenic properties, yet it is limited due to donor site morbidity and inadequate availability.[5] Alternative options, including the use of allografts or xenografts,[6] raise major concerns associated with bioactivity decrease, possible immunogenicity, increased risk of disease transfer and infections, and a high cost of sample preparation, handling and storage.[7-9] To overcome these limitations, bone tissue engineering has been proposed as an alternative therapeutic approach aimed at simulating the natural state of bone tissue and its surrounding microenvironment. This approach is based on *in vitr*o formation of engineered graft materials to be clinically used for reconstruction of bone defects *in vivo*. The basic elements of bone tissue-engineering include a scaffold material which serves as an artificial extracellular matrix (ECM), stem cells, and osteoinductive growth factors.[10] The scaffold material needs to be integrated into the surrounding bone tissue and provide a three-dimensional (3D) framework for cell adherence. It should thus be biocompatible, biodegradable, and have the appropriate mechanical strength at the time of implantation while withstanding degradation. Finally, it should enable the normal physiological repair process of damaged tissue.[11]

The tissue-mimicking nanotopography of the scaffold, including both its chemical composition and physical properties (shape, surface, and stiffness), has a crucial effect on stem cell responses, such as adhesion, migration and differentiation, resulting in better implant-tissue integration.[12-19]

Various scaffold materials are utilized in bone tissue engineering applications. Hydrogels, either synthetic or natural in composition, are frequently used as ECM-mimicking scaffolds for cell growth due to their hydrophilic nature and capacity to absorb several fold their dry weight in water, allowing cells to adhere and differentiate onto their matrices.[20-22] Specially, natural polysaccharide hydrogels have been frequently investigated for tissue engineering purposes due to their inherent biocompatibility, high water content, and molecular structure, which is similar to that of the natural ECM.[23-25] These properties render them easily biodegradable and favorable for cell incorporation and migration. However, they are not commonly implemented for bone regeneration due to their low mechanical properties compared to those of the natural bone.[26] Consequently, the use of synthetic biomaterials hydrogels with controllable and reproducible properties is appealing for bone tissue engineering.[27]

Short peptides can be used as low molecular weight gelators and form mechanically stable hydrogels through self-assembly into supramolecular structures,[28-34] which typically arise from non-covalent interactions, such as hydrogen-bonding, van der Waals interactions, π–π stacking and electrostatic interactions.[35-37] Furthermore, the material properties can be tailored to form multi-component supramolecular gels which can be composed of: (1) two components which do not form a gel on their own, (2) two or more gelators which can either co-assemble or self-sort into distinct assemblies, (3) one or more gelator and one or more non-gelling additive which can affect the assembly process of the gelator.[38-41] Controlling the properties of the resulting gels is achieved by different interactions and by changing the ratio of the different components, enabling to modulate cellular functionality and tissue morphogenesis.[39, 42]

Fluorenyl-9-methoxycarbonyl (Fmoc)-functionalized peptides are of the most studied low molecular weight gelators. One notable example is Fmoc-diphenylalanine (FmocFF) that can

form a rigid hydrogel without a need for an additional crosslinking agent,[43] resulting in a biocompatible gel network that mimics the ECM. The properties of this dipeptide hydrogel can be easily modified by changing the amino acids sequence and the aromatic N-terminus groups.[32, 44] Incorporation of inorganic materials such as hydroxyapatite (HAP) into hydrogel matrices has been shown to support the cellular growth of human osteoblast,[45] enhance bone mineralization by forming nucleation sites,[46, 47] as well as to support angiogenic and osteogenic activity in collagen scaffolds after subcutaneous ectopic implantation in mice.[48] HAP is easily dissolved, forming a high calcium ion layer and a slightly alkaline environment, which can effectively promote osteoblast adhesion, proliferation and matrix secretion, thus improving the mechanical properties of the composite material.[49]

Peptides and amino acids play an important role in biomineralization.[50, 51] Specifically, the interaction between $Ca^{2+}$ and $PO_4^{3-}$ with both negative and positive charged amino acids glutamate and arginine, respectively, to form HAP aggregates and later give rise to HAP crystals has been shown by Cerruti and colleagues.[51] In addition, arginine has been shown to increase bone mineral density by stimulating growth hormone production.[50] Moreover, it is considered to be one of the most essential amino acids for young developing mammals, suggesting a role for arginine in tissue development.[52] Brasinika *et* al. demonstrated enhanced human mesenchymal stem cells attachment, proliferation, and differentiation on HAP surfaces in the presence of collagen and arginine.[53] The addition of arginine can also be used as a strategy to fine-tune the bioactivity of the HAP crystals, as previously suggested.[54, 55]

In the present study, we designed peptide-based multi-component hydrogels composed of two building blocks, FmocFF and Fmoc-arginine (FmocR). We allowed the hydrogels to form at different ratios of the building blocks in order to modulate the hydrogel physical properties. In

addition, we incorporated HAP within the hydrogels to form 3D scaffolds for bone tissue regeneration. We characterized the multi-component hydrogels secondary structure, their mechanical properties, and biocompatibility. An optimum composition of FmocFF, FmocR and HAP resulted in a superior rigid and biocompatible hybrid suitable for cell adhesion hence applicable in the future as a bone tissue engineering scaffold.

## Experimental Section

**Materials.** Lyophilized Fmoc-Phe-Phe-OH (FmocFF) and Fmoc-Arg-OH (FmocR) were purchased from Bachem (Budendorf, Switzerland) and Sigma Aldrich (Rehovot, Israel), respectively. HAP nanoparticles were synthesized by a wet precipitation method in an aqueous system and have been previously shown to be pure HAP particles with an ellipsoidal shape and an average size of approximately 80 nm, without heterogeneous phases.[46]

**Formation of the hydrogels.** FmocFF and FmocR solutions were prepared separately by dissolving the powders to a concentration of 100 mg/mL in dimethyl sulfoxide (DMSO) and vortexed until the solution became transparent. Single peptide solutions were prepared by adding 50 μL of the aqueous stock solutions to 950 μL double distilled water over vortex. FmocFF:FmocR mixed solutions at a final concentration of 5 mg/ml were prepared by combining the two peptides stock solutions in DMSO at the desired molar ratios of 3:1 (37.5 μL and 12.5 μL), 1:1 (25 μL and 25 μL) and 1:3 (12.5 μL and 37.5 μL), respectively. The mixed solutions were then diluted in 950 μL double distilled water and vortexed. For the HAP-incorporated hydrogels, 1 mg/mL HAP was dispersed in 950 μL of DDW by sonication in 0-4°C to avoid sample heating. Pure FmocFF and FmocR and their mixed stock solutions were then added to the HAP aqueous solution with vortex mixing using the ratios detailed above.

**Absorbance kinetics analysis**. Samples of 150 μL were taken into a 96-well plate. Absorbance at 400 nm, 500 nm and 600 nm was measured every 5 min using a TECAN Infinite M200PRO plate reader, for a total of 24 h.

**Transmission electron microscopy (TEM).** Samples (10 μL) of FmocFF, FmocR, and hybrids were prepared for TEM analysis (Electron Microscopy Sciences LTD). The excess liquid was removed 2 minutes later using cellulose filter paper. 10 μL of 2% uranyl acetate was then deposited on the grid and allowed to adsorb for 2 min before excess fluid was blotted off. Prior to analyses, samples were left to air dry at ambient conditions. TEM analysis was performed using a JEM-1400Plus Transmission Electron Microscope (JEM), operating at 80 kV.

**EDX analysis using high resolution scanning electron microscopy (HR-SEM).** Hydrogel samples were placed on glass slides and left to air dry at ambient conditions. The samples were then coated with Cr for conductance and viewed and analyzed using a JSM-6700 field-emission HR-SEM (JEOL, Tokyo, Japan), equipped with a cold field emission gun, operating at 10 kV.

**Rheological analysis.** Rheological measurements were performed using an AR-G2 controlled-stress rheometer (TA Instruments, USA). Time-sweep oscillatory tests in parallel plate geometry were performed on 250 μL of fresh solution (resulting in a gap size of 0.6 mm), at room temperature. Oscillatory strain (0.01-100%) and frequency sweeps (0.01-100 Hz) were conducted in order to determine the linear viscoelastic region, at which the time sweep oscillatory tests were performed. G' and G", the storage and loss moduli, respectively, were obtained at 5 Hz oscillation and 0.5% strain deformation for each sample.

**Fluorescence spectroscopy.** The emission spectra of the gels were recorded using a Horiba JobinYvon FL3-11 fluorimeter (Horiba JobinYvon, NJ, USA). A quartz cuvette with an optical

path length of 1 cm was used. The gels were assembled within the cuvette and the spectrum was collected. The experiments were carried out using an excitation wavelength of 280 nm and 5 nm excitation and emission slits.

**Fourier-Transform Infrared (FTIR) spectroscopy**. FTIR spectra were collected 4 days after gel preparation using a Nicolet Nexus 470 FTIR spectrometer with a DTGS (deuterated triglycine sulfate) detector. Hydrogels samples were placed onto disposable KBr IR sample cards (Sigma-Aldrich, Israel) and vacuum dried. Measurements were performed using $4cm^{-1}$ resolution and by averaging 2000 scans. The absorbance maxima values were determined using the OMNIC analysis program (Nicolet). The obtained transmittance spectra were smoothed by applying the Savitzky-Golay function to eliminate noise and operating the second derivative transformation on the spectra using the Peakfit software version 4.12 (SYSTAT Software Inc., Richmond, CA).

**Cell viability analysis.** 3T3 mouse fibroblast cells were purchased from ATCC and cultured in Dulbecco's Modified Eagle's Medium (DMEM) supplemented with 10% fetal calf serum, 100 U $mL^{-1}$ penicillin, 100 U $mL^{-1}$ streptomycin, and 2 mmol $L^{-1}$ L-glutamine (all from Biological Industries, Israel). The cells were maintained in a petri dish at 37 °C in a humidified atmosphere containing 5% $CO_2$. Gels were formed in a 24 well-plate and repeatedly washed for 3 days with culture medium to ensure complete removal of excess materials and solvent followed by UV sterilization. Subsequently, the pH of the final medium over the gels was measured to be 7.4-7.8, as also inferred from the medium color, which was observed to be the same as that of the naïve medium, indicating a suitable pH required for cell culture. After reaching a confluence of 90%, the cells were separated from the petri dish using trypsin A and 60,000 cells in 0.1 ml of fresh culture medium were seeded per well, on the pre-washed gel samples, and incubated for 8 hours.

A fluorescent live-dead staining assay (Sigma Aldrich) containing fluorescein diacetate (6.6 μg/ml) and propidium iodide (5 μg/ml) was then used to visualize the proportion of viable versus non-viable cells. The labelled cells were immediately viewed using a Nikon Eclipse Tifluorescent microscope and images were captured by a ZylascMOS camera using Nikon Intensilight C-HGFI fluorescent lamp.

## Results and Discussion

**Formation of multi-component hydrogels decorated with hydroxyapatite.** To form multi-component hydrogels that can anchor HAP to serve as 3D scaffolds for bone tissue regeneration, we prepared two component hydrogels using FmocFF and FmocR (Figure 1a). Pure FmocFF forms a stable gel at room temperature by the solvent switch method in 5% DMSO/water solvent mixture (Figure 1b).[56] However, pure FmocR did not form hydrogels in all the conditions tested in this study (Figure 1b). Herein, we generated multi-component hydrogels composed of FmocFF, which forms a stable fibril network-based hydrogel, and FmocR, that allows the anchoring of HAP.[50] We combined FmocFF and FmocR at different ratios of 3:1, 1:1 and 1:3. All hybrid hydrogels were prepared by the solvent switch method in DMSO/water medium at an overall DMSO concentration of 5%. Inverted vials of the five samples are shown in Figure 1b, demonstrating that FmocFF, as well as the multi-component hydrogels, form stable hydrogels. The FmocFF hydrogel is transparent, however the elevation in FmocR ratio in the hybrid solutions resulted in increased turbidity (Figure 1b). The majority of scaffolds that are currently used for bone tissue regeneration are polymer-ceramic composites.[27] The incorporation of inorganic HAP crystals into organic scaffolds has led to successful results in bone regeneration, probably due to the positive effect of HAP on the scaffold's mechanical properties.[57]

Nevertheless, the homogeneous integration of these particles into the hydrogel scaffold is a challenging task. We utilized the affinity of arginine to HAP[50] in order to homogeneously incorporate HAP within our multi-component hydrogels. HAP at a concentration of 1 mg/ml was incorporated within the aqueous phase prior to the solvent switch step using sonication to form an organic-inorganic scaffold (Figure 1c). To quantify the kinetics of the gelation process, we monitored the absorbance at 400 nm over time. While the absorbance of the FmocFF solution decreased within 2 minutes, reaching an optical density (OD) of 0.4 AU, the hybrid hydrogels showed slower kinetic profiles. FmocFF:FmocR 3:1 and 1:1 formed a clear hydrogel after 40 and 110 mins with OD of 0.26 AU and 0.44 AU, respectively (Figure 1d). However, the FmocFF:FmocR 1:3 hybrid formed a clear hydrogel in a significantly longer time of ~280 mins, reaching an OD of 0.76 AU. The absorbance results show that the increase in FmocR ratio in the hybrid hydrogels resulted in a prolonged gelation time, as well as higher hydrogels absorbance. Interestingly, the addition of HAP to the hydrogels accelerated their gelation process, as minimum absorbance was achieved after a shorter time (Figure 1e). This might be due to the ability of the HAP particles to serve as nucleation sites facilitating the self-assembly process which accelerates hydrogel formation.

FmocFF:FmocR 3:1-HAP formed transparent hydrogel after 15 mins with OD of 0.25 AU, while FmocFF:FmocR 1:1-HAP and FmocFF:FmocR 1:3-HAP formed transparent hydrogel after 45 mins (OD of 0.3 AU) and 110 mins (OD of 0.7 AU), respectively (Figure 1e). The decreased duration of the gelation process may be attributed to the presence of HAP as an accelerating factor in the gelation process. Previous studies have shown that additives can enhance the mechanical strength of FmocFF and affect its gelation time. For example, the addition of a polysaccharide, konjac glucomannan, decreased the gelation time and led to higher

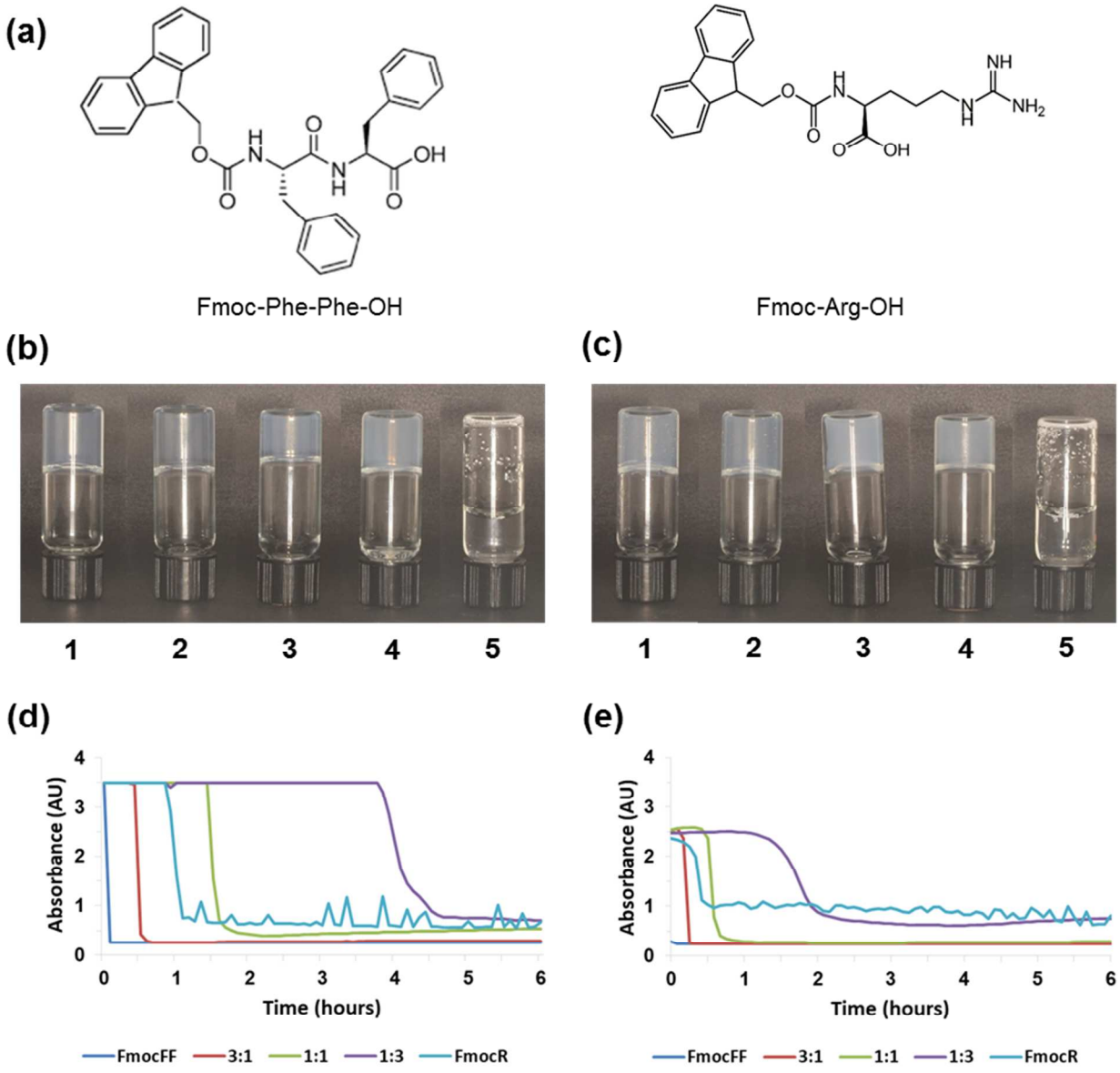


**Figure 1. Hydrogels gelation kinetics.** (a) Molecular structure of the two building blocks, FmocFF and FmocR. (b) Inverted vials of the single and hybrid hydrogels and (c) inverted vials of the different hydrogels incorporated with HAP: (1) FmocFF, (2) FmocFF:FmocR 3:1, (3) FmocFF:FmocR 1:1, (4) FmocFF:FmocR 1:3, (5) FmocR. (d) Absorbance changes of the hydrogels over time (absorbance at 400 nm). (e) Absorbance changes of the HAP containing hydrogels over time (absorbance at 400 nm).

stability and higher mechanical strength,[58] and the addition of sodium alginate to FmocFF improved the stability of the FmocFF hydrogel.[59] In contrast, the addition of dextran to FmocFF resulted in gels with lower rheological properties.[60]

The kinetic profiles of the hydrogels show that with the increase in FmocR fraction in the various HAP-incorporated hybrid hydrogels the end point absorbance is lower. This observation can indicate the inclusion of HAP to arginine, leading to its homogenous dispersion in the hydrogel that affect the hydrogel absorbance (Figure 1e). Similar to the absorbance measurements at 400 nm, the analysis was also performed at 500 nm and 600 nm. No significant differences were observed between the different wavelengths (Figure S1).

**Ultrastructural analysis of the multi-component hydrogels.** To examine the hydrogel underlying morphologies, we used TEM analysis. TEM samples were prepared for all the multi-component hydrogels with and without HAP, as well as for the pure FmocFF hydrogel and FmocR (Figure 2). FmocFF, FmocFF:FmocR 3:1 and FmocFF:FmocR 1:1 hydrogels were comprised of long entangled fibrils, several micrometers long (Figure 2a, c, e and Figure S2a, c, e). The HAP incorporated hydrogels FmocFF-HAP, FmocFF:FmocR 3:1-HAP and FmocFF:FmocR 1:1-HAP also showed similar fibrils formation (Figure 2b, d, f and Figure S2b, d, f). In addition, in the HAP containing hydrogels, the presence of HAP nanoparticles in between the fibrils was visible as needle-like structures. Interestingly, FmocFF:FmocR 1:3 and FmocFF:FmocR 1:3-HAP hydrogels showed fewer fibrils which are relatively less entangled, suggesting a lower hydrogel formation capability (Figure 2g, h, S2g, h). In the pure FmocR solution, which does not form gel, spherical assemblies were observed both with and without HAP (Figure 2i, j). However, no such spherical structures were observed in the hybrid multi-component hydrogels. To further quantify the presence of HAP particles in the multi-component hydrogels, we performed energy-dispersive X-ray spectroscopy (EDX) analysis in high resolution scanning electron microscopy (HRSEM).

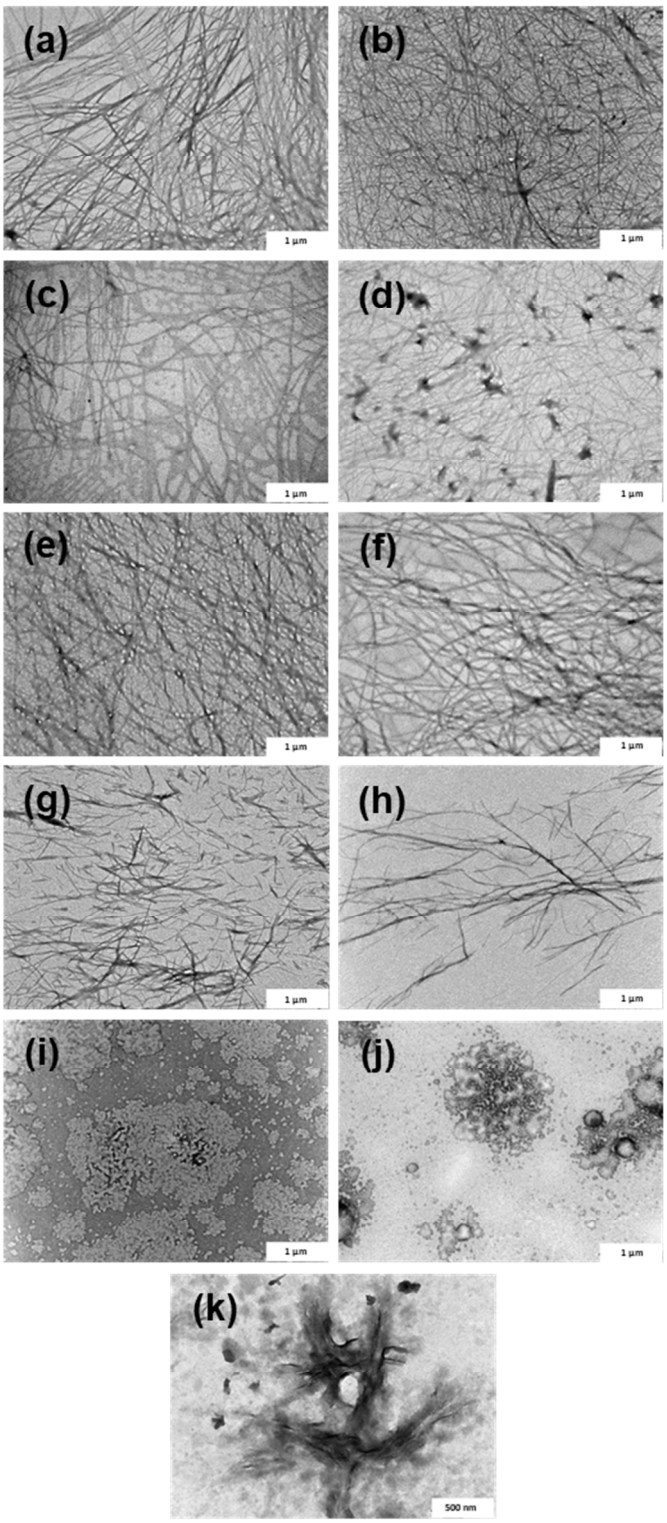


**Figure 2. TEM images of the studied hydrogels.** (a) FmocFF, (b) FmocFF-HAP, (c) FmocFF:FmocR 3:1, (d) FmocFF:FmocR 3:1-HAP, (e) FmocFF:FmocR 1:1, (f) FmocFF:FmocR 1:1-HAP, (g) FmocFF:FmocR 1:3, (h) FmocFF:FmocR 1:3-HAP, (i) FmocR, (j) FmocR-HAP, (k) HAP nanoparticles. Scale bar for (a-j) is 1 µm, Scale bar for (k) is 500 nm.

242 FmocFF-HAP and FmocFF:FmocR 3:1-HAP hydrogels were analyzed and the measured

presence

**Table 1:** EDX elemental analysis of FmocFF-HAP hydrogel.

| Element line | Element Wt% | Wt% Error |
|---|---|---|
| C K | 55.41 | ±1.07 |
| O K | 42.97 | ±2.85 |
| Ca K | 1.61 | ±0.55 |
| Total | 100 | |

**Table 2:** EDX elemental analysis in FmocFF:FmocR 3:1-HAP hybrid hydrogel.

| Element line | Element Wt% | Wt% Error |
|---|---|---|
| C K | 29.48 | ±2.47 |
| O K | 66.28 | ±4.29 |
| Ca K | 4.24 | ±0.56 |
| Total | 100 | |

of calcium was 1.61 wt% (Table 1) and 4.24 wt%, respectively (Table 2). This higher percentage of calcium in the multi-component hydrogels demonstrates that the arginine moiety indeed supports the incorporation of HAP particles into the hydrogel (Table 1-2).

**FTIR analysis of the multi-component hydrogels.** FTIR analysis was further used to understand the secondary structure of the building blocks that form the multi-component hydrogels. Examining the amide I region of the FTIR transmittance spectra of all the multi-component hydrogels, namely FmocFF:FmocR 3:1, FmocFF:FmocR 1:1, FmocFF:FmocR 3:1-HAP and FmocFF:FmocR 1:1-HAP, we observed a distinct peak at 1690 $cm^{-1}$ suggesting both

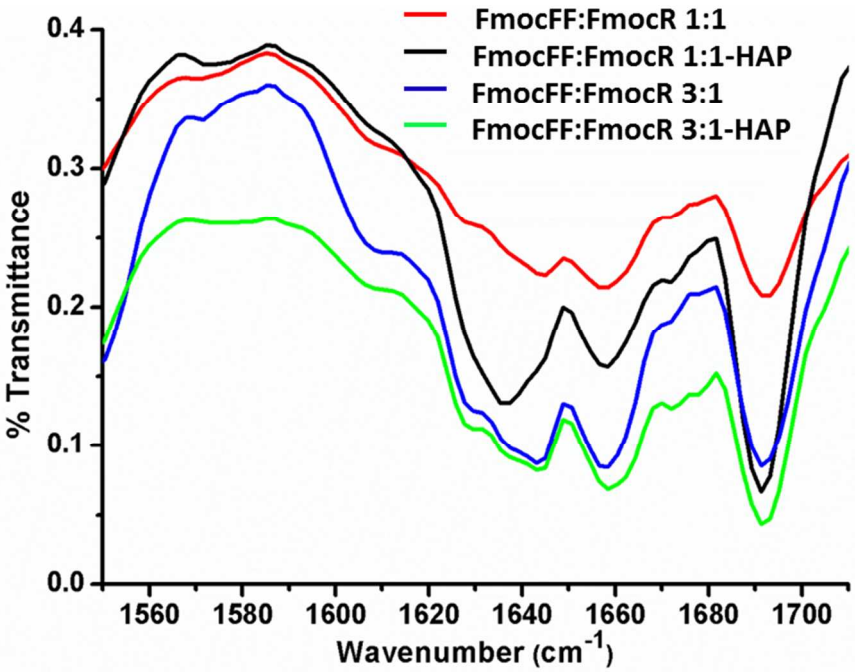


**Figure 3. FTIR analysis of the studied hydrogels.** FTIR spectra in the amide I region of the multi-component hydrogels showing distinct peaks in the range of 1635-1645 $cm^{-1}$ indicating β-sheet structures, and at 1690 $cm^{-1}$ indicating both β-sheet structures and carbamate moiety of FmocFF.

the presence of a carbamate moiety and that the hybrid hydrogels are rich in β-sheet (Figure 3).[44, 61, 62] An additional peak was observed between 1635 and 1645 $cm^{-1}$ in all the multi-component hydrogels, also confirming the β-sheet structure (Figure 3). Similarly, peaks at 1690 $cm^{-1}$ and 1640 $cm^{-1}$ were observed for the pure FmocFF hydrogel (Figure S3). Such β-sheet secondary structures are probably due to the Fmoc-amino acid moiety which forms π- π stacking interactions.[44, 63] However, no such peak was observed in the spectrum of FmocR, probably because it does not assemble nor forms a gel (Figure S3).

**Rheological characterization.** To investigate the effects of each building block on the viscoelastic properties of the multi-component gels, we performed rheological analysis.[64] First, dynamic frequency sweep (at 0.1% strain) and strain sweep (at 1 Hz) oscillatory measurements were performed in order to optimize the appropriate measurement conditions. The frequency sweep experiments using a frequency range of 0.1-100 Hz showed a wide linear viscoelastic

region in the FmocFF and the multi-component FmocFF:FmocR 3:1, 1:1 hydrogels (Figure S4a, c, d).

**Table 3: Viscoelasticity analyses of the hydrogels.**

| | Storage modulus (G') (Pascal) | Loss modulus (G'') (Pascal) | Tan δ | Breakage Strain (%) |
|---|---|---|---|---|
| FmocFF | 6413 | 325 | 0.053 | 52 |
| FmocFF-HAP | 12151 | 670 | 0.052 | >100 |
| FmocFF:FmocR 3:1 | 4988 | 172 | 0.034 | 46 |
| FmocFF:FmocR 3:1-HAP | 29172 | 912 | 0.024 | ~100 |
| FmocFF:FmocR 1:1 | 636 | 42 | 0.037 | 23 |
| FmocFF:FmocR 1:1-HAP | 15867 | 583 | 0.031 | 76 |
| FmocFF:FmocR 1:3 | 57 | 5 | 0.065 | 13 |
| FmocFF:FmocR 1:3-HAP | 1176 | 77 | 0.066 | 52 |

To analyse the effect of oscillatory strain on the different hydrogels, they were subjected to 0.01-100% strain sweep (Figure S5). FmocFF as well as the multi-component FmocFF:FmocR 3:1, 1:1, and 1:3 hydrogels showed a LVR of up to 1% strain (Figure S5a, c-e). Furthermore, we studied the breakage strain of all the hydrogels. The breakage strain of FmocFF was 52% (Table 3). In the multi-components gels, breakage strain values of 46%, 23%, 13% were found in the FmocFF:FmocR 3:1, 1:1, 1:3 hydrogels, respectively (Table 3). In the presence of HAP, these values increased to >100% in FmocFF and 100%, 76%, 52% in FmocFF:FmocR 3:1, 1:1, 1:3 hydrogels, respectively (Table 3). This increase in the breakage strain values in the presence of HAP demonstrates its contribution to the mechanical strength of the hydrogels. In FmocR, however, as in the frequency sweep experiments, no difference was found between G' and G'', probably because of its inability to form a gel.

Based on the frequency sweep and oscillatory strain sweep analysis, the *in situ* kinetics of hydrogels formation and their mechanical properties were characterized at a fixed strain of 0.5% and a frequency of 5 Hz over 1h (Figure 4a, and Figure S6). The rheological analysis of the multi-component hydrogels showed endpoint storage modulus values of 4988, 636 and 57 Pa for the multi-component FmocFF:FmocR 3:1, 1:1 and 1:3, respectively, whereas pure FmocFF showed a storage modulus value of 6,413 Pa (Figure 4), consistent with the decreased hydrogels rigidity as the fraction of FmocR increases. Time sweep of FmocFF, FmocFF:FmocR 3:1, FmocFF:FmocR 1:1 hydrogels showed a storage modulus (G') that is considerably higher than the loss modulus (G''), indicating a gel phase (Figure S6a,c,d). However, in the multi-component FmocFF:FmocR 1:3 hydrogel only a slight difference was found between G' and G'', indicating a weak gel formation (Figure S6e). Even slighter difference was found in the FmocR, in correlation to its inability to form gel (Figure S6b). In the presence of HAP, higher differences were found between G' and G'' in FmocFF as well as in all the multi-component hydrogel systems (FmocFF:FmocR 3:1, 1:1, and 1:3) (Figure S6a, c-e). These differences were higher with the increase in FmocFF percentage in the multi-component hydrogels (FmocFF:FmocR 3:1>1:1>1:3) (Figure S6c-e). The higher differences found in the HAP incorporated gel systems when compared to these without HAP may suggest its strengthening effect on the resulting gels. The weak hydrogel obtained for the multi-component FmocFF:FmocR 1:3 is in accordance to the TEM analysis showing short entanglement-free fibrils (Figure 2g). Interestingly, in FmocFF and FmocFF:FmocR 3:1, a significant portion of the gel rigidification is achieved within less than 4 mins, while the gelation of FmocFF:FmocR 1:1 takes approximately 30 mins (Figure 4a). However, the point where the gelation process and rigidification are complete, i.e. the time in which the storage modulus G' reaches its plateau, is a much longer process. The pure FmocFF

hydrogel exhibited a G' maximum value after a short gelation time of approximately 15 mins (Figure 4a), while the FmocFF:FmocR 3:1 showed a gelation time of about 26 mins. The multi-component FmocFF:FmocR 1:1 hydrogel reached a maximum G' value after 40 mins. Moreover, hydrogels may be more relevant for tissue-engineering applications if their mechanical rigidity is in the range of kPa, since it has been previously reported that stem cells go through stiffness-directed differentiation into neuronal, chondrogenic, and osteogenic fate on soft, stiff and rigid hydrogels, respectively.[65-67]

In addition to its importance as the main mineral in bone tissue regeneration, here we demonstrated that the addition of HAP also reinforce the mechanical rigidity of the hybrid hydrogels. The storage modulus of the FmocFF-HAP hydrogel was found to be almost two times higher than that of the pure FmocFF hydrogel. The rheological analysis demonstrated that the FmocFF-HAP hydrogel gelation process starts within 4 mins and reaches rigidity after approximately 15 mins with a final storage modulus of 12,151 Pa (Figure 4a), confirming that the incorporation of HAP particles enhances the rigidity of the hydrogel. As for the multi-component FmocFF:FmocR 3:1 and 1:1 hydrogels, the addition of HAP enhanced their mechanical rigidity by almost 5 and 24 fold, reaching values of 29,172 and 15,867 Pa, respectively, after 1h (Figure 4b). However, even in the presence of HAP the mechanical rigidity of the multi-component FmocFF:FmocR 1:3 hydrogel was low compared to the other hydrogels. This HAP-incorporated hydrogel was formed only after approximately 2h, reaching a rigidity of 1,176 Pa, compared to 57 Pa in the absence of HAP (Figure S1, and Figure 4b). Probably due to less entangled network in the FmocFF:FmocR 1:3 as observed from TEM images, HAP particles are not well integrated in the network compared to those of the 3:1 and 1:1 hydrogels, which is reflected in the mechanical rigidity of the HAP included hydrogels. The loss factor, tan δ,

defined as G''/G', was calculated for all hydrogel systems (Table 3). In all cases, δ values were in the range 0.02-0.06, i.e. less than 1, indicating gel formation.[68, 69]

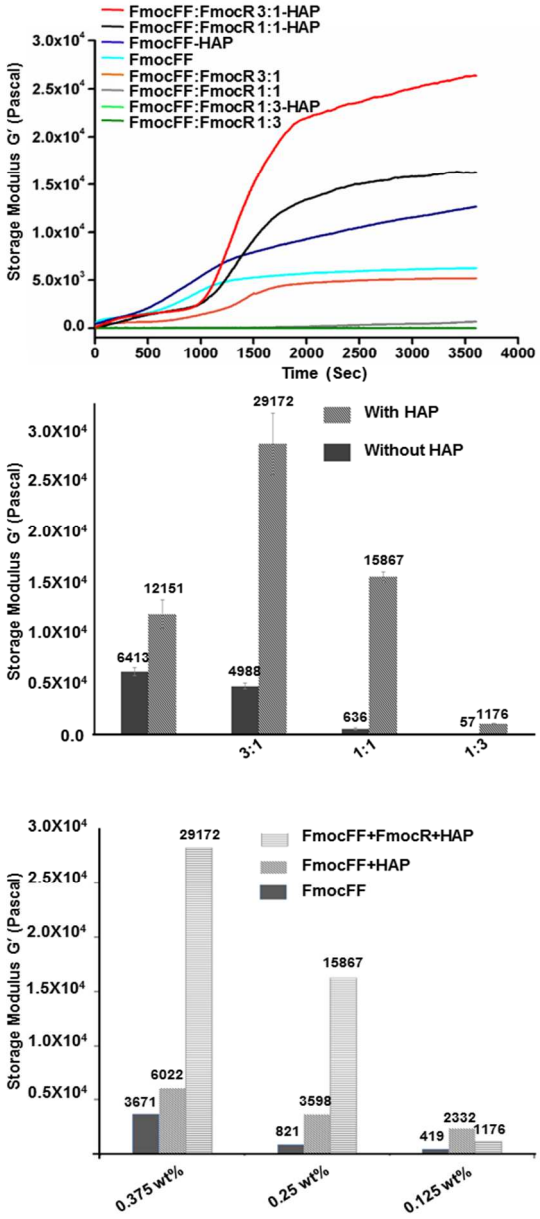


**Figure 4. Rheological analysis of hydrogels.** (a) *In situ* time sweep oscillation measurements of pure FmocFF and multi-component FmocFF:FmocR 3:1, FmocFF:FmocR 1:1 and FmocFF:FmocR 1:3 hydrogels formation, with and without HAP. (b) Comparative study of the end point storage modulus (G') in time sweep rheology of the hydrogels (the value of mechanical storage modulus at 1h for FmocFF, 3:1, 1:1 with and without HAP, 12h for 1:3 without HAP and 6h for 1:3 with HAP). (c) Comparative study of the end point storage modulus (G') in time sweep rheology of pure FmocFF at different concentrations and the different multi-component hydrogels with and without HAP (the value of mechanical storage modulus at 1h for FmocFF, 3:1, 1:1 with and without HAP, 12h for 1:3 without HAP and 6h for 1:3 with HAP).

328

In order to examine whether the improved mechanical rigidity of the multi-component hydrogels can be attributed to a possible co-assembly between FmocFF and FmocR or solely to the different concentrations of FmocFF in the various multi-component hydrogels, we performed time sweep analyses of FmocFF hydrogels at the different concentrations present in the multi-component hydrogels, with and without HAP. G' values of 3671, 821 and 419 Pa were observed for the pure 0.375 wt%, 0.25 wt% and 0.125 wt% FmocFF hydrogels, respectively (Figure S7). Although higher values of 6022, 3598 and 2332 Pa were observed for the HAP-incorporated hydrogels, respectively, they were still significantly lower than those of the corresponding HAP-incorporated multi-component FmocFF:FmocR systems. These results suggest that FmocR plays a crucial role in the overall mechanical rigidity of the HAP-incorporated multi-component FmocFF:FmocR 3:1 and 1:1 hydrogels. This effect can be attributed to a co-assembly process between FmocFF and FmocR and to an increased binding of HAP particles to FmocR. However, this synergistic effect between HAP and the mixed FmocFF:FmocR was not observed in the multi-component FmocFF:FmocR 1:3 hydrogel, possibly due to a less entangled network that did not allow homogeneous integration of the HAP particles, as suggested above.

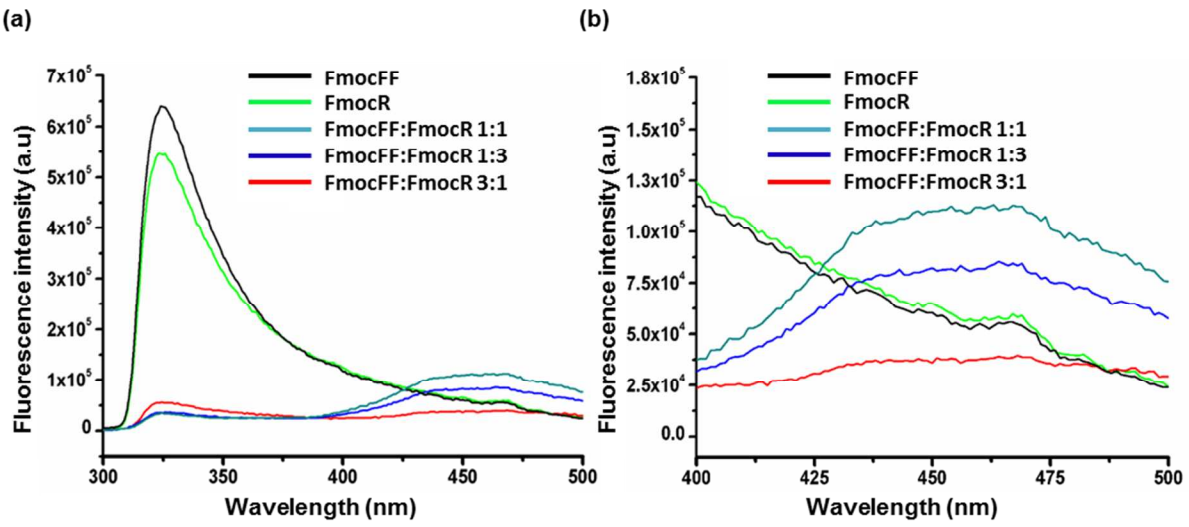


**Figure 5.** Fluorescence emission spectra of the multi-component hydrogels at an excitation of 300-500 nm.

**Fluorescence spectroscopy.** The photoluminescence study of the hydrogels formation is shown in Figure 5. FmocFF and FmocR show a peak at 320 nm characteristic of the fluorenyl peak (Figure 5a). A broad peak in the range of 440-470 nm were observed for the multi-component FmocFF:FmocR 3:1, 1:1, 1:3 hydrogels and were not observed for the individual building blocks, suggesting a co-assembly mechanism of the two component. Fmoc-protected hydrogelators, as suggested previously for the hydrogel formation by a co-assembled system of Fmoc-tyrosine and Fmoc-arginine (Figure 5b).[41, 70]

**Cytocompatibility of the HAP-incorporated multi-component hydrogels.** In order to examine whether the newly formed hydrogels can serve as scaffolds for bone tissue engineering applications, their biocompatibility was examined using *in vitro* cellular analysis. As discussed in the experimental section, gels were formed in a 24 well-plate and repeatedly washed for 3 days with culture medium to ensure complete removal of excess materials and solvent followed by UV sterilization. The pH of the gels after washing was found to be 7.4-7.8.

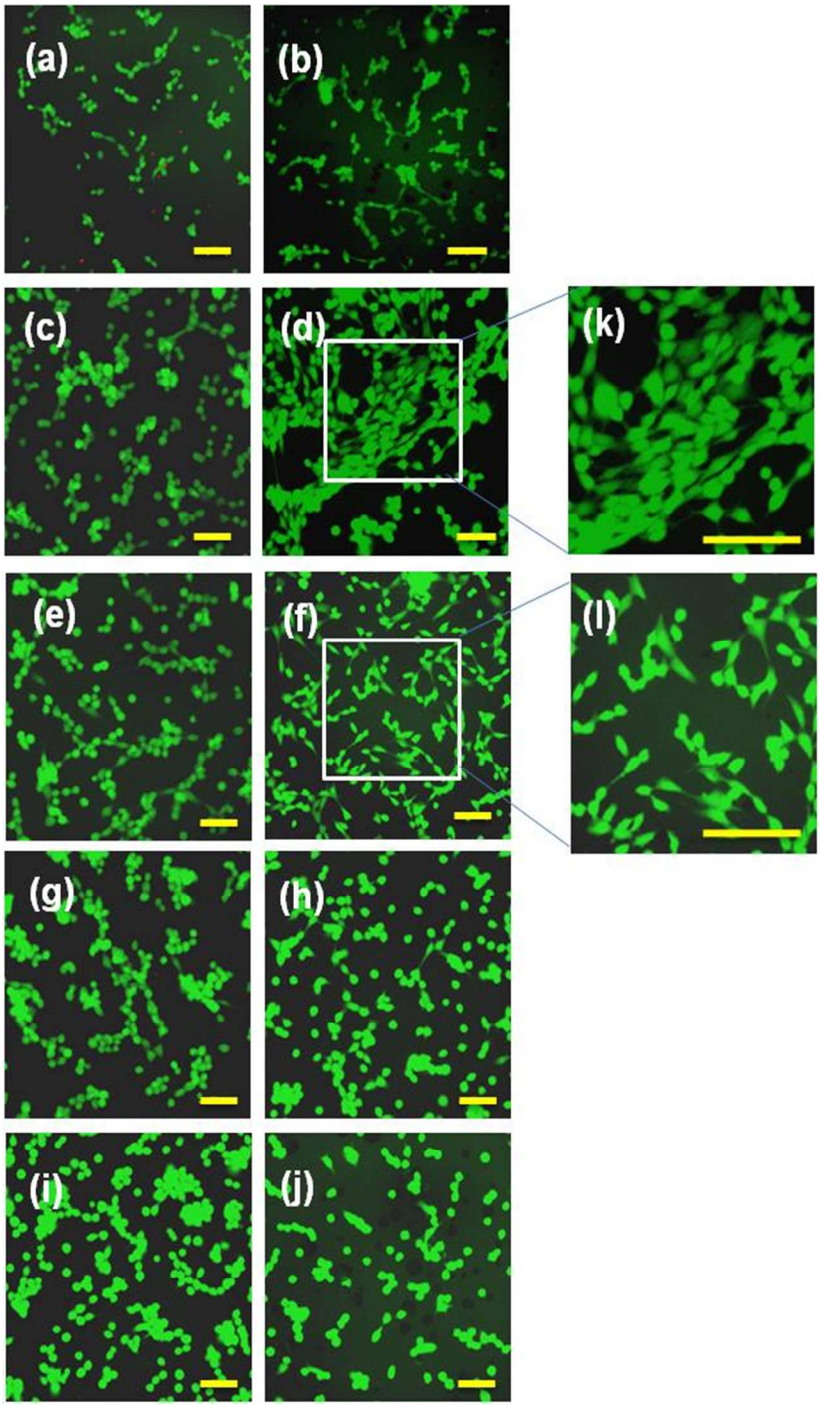


**Figure 6.** Live-dead staining of 3T3 fibroblasts culture after 8 h treatment with: (a) FmocFF, (b) FmocFF-HAP, (c) FmocFF:FmocR 3:1, (d) FmocFF:FmocR 3:1-HAP, (e) FmocFF:FmocR 1:1, (f) FmocFF:FmocR 1:1-HAP, (g) FmocFF:FmocR 1:3, (h) FmocFF:FmocR 1:3-HAP, (i) FmocR, (j) FmocR-HAP. Magnified insets of cells grown on (k) FmocFF:FmocR 3:1-HAP and (l) FmocFF:FmocR 1:1-HAP gels. Green staining indicates live cells, red staining indicates dead cells. Scale bar is 500 μm.

358

The Mouse Swiss Albino Embryo Fibroblast cells (3T3) were seeded on the hydrogels following their formation in a 24-well culture plate. Eight hours later the cells were analyzed for viability using live-dead staining with fluorescein diacetate, a cell membrane dye indicating live cells (green), and the propidium iodide, a DNA stain indicating dead cells (red). Figure 6 shows sufficient population of green cells on all the hybrid hydrogels with and without HAP. In addition, no propidium iodide, staining can be detected implying that the hydrogels support the viability of 3T3 cells. However, few red stained cells are observed in the presence of the pure FmocFF gel (Figure 6a), indicating few dead cells. Regarding cell morphology, round green cells with nonspecific morphological characteristics were observed on FmocFF and FmocFF-HAP hydrogels (Figure 6a-b), suggesting the pure FmocFF hydrogel did not support cell adherence. Similar round green cells were observed on the FmocFF:FmocR 3:1 and 1:1 hybrid hydrogels, which can be attributed to their inadequate mechanical rigidity to support 3T3 cells adhesion (Figure 6c, e). Interestingly, on FmocFF:FmocR 3:1-HAP and FmocFF:FmocR 1:1-HAP, a large population of adherent green cells could be observed (Figure 6d, f, k, l).This observation may be attributed to an optimum concentration of the building blocks enabling these hybrid hydrogels to fulfil the required rigidity for both cell attachment and mechanical support, which could be utilized for cell proliferation and differentiation applications.[71-74]

## Conclusions

This study demonstrates the formation of hydrogel networks with enhanced bio functionality facilitated by co-assembly of FmocFF and FmocR. The FmocFF peptide contributes to stabilization of the hydrogel while FmocR displays the arginine side chain that has high affinity to HAP particles. Furthermore, the novel HAP-incorporated self-assembled hydrogels are

composed of a nanometric fibril network that displays a β-sheet secondary structure conformation. In addition, these hydrogels demonstrate remarkable mechanical rigidity of up to 29 KPa for the FmocFF:FmocR 3:1-HAP hydrogel. These novel multi-component organic-inorganic peptide-based hydrogels can serve as potential components of scaffolds for bone tissue-engineering due to their enhanced mechanical properties and the presence of calcium bone particles, along with improved cell adhesion and viability.

**Associated contents**

**Supporting Information (S)**

The Supporting Information is available free of charge on the ACS Publications website. Supporting information includes hydrogels gelation kinetics, TEM images of the studied hydrogels, FTIR spectra, as well as comprehensive rheological analysis of the gels.

**Acknowledgements**

The authors are grateful to Dr. Zahava Barkay and Noam Brown for help with EDX analysis, Dr. Vered Holdengreber for assistance with TEM analysis and Dr. Sigal Rencus-Lazar for linguistic editing. This study was supported by the Ministry of Science, Technology & Space, Israel. The authors also thank the members of the Adler-Abramovich group for helpful discussions.

# Table of contents

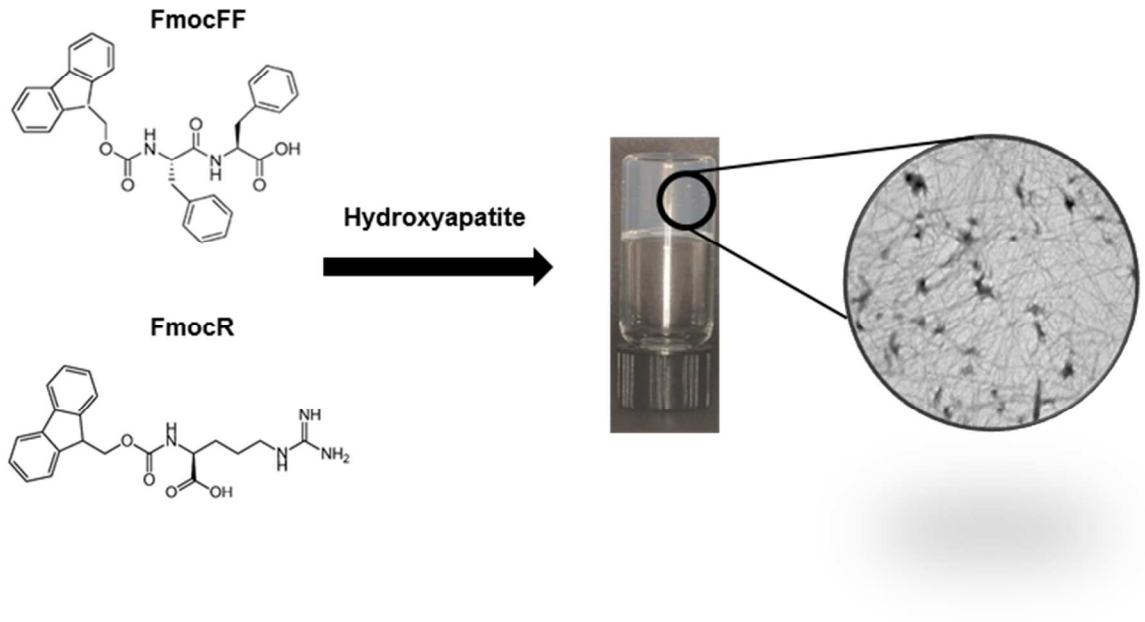

## References


1. Currey, J. D. How well are bones designed to resist fracture? *J. Bone Miner. Res.* **2003,** *18*, 591-598.
2. Reznikov, N.; Shahar, R.; Weiner, S. Bone hierarchical structure in three dimensions. *Acta Biomater.* **2014,** *10*, 3815-3826.
3. Petite, H.; Viateau, V.; Bensaid, W.; Meunier, A.; de Pollak, C.; Bourguignon, M.; Oudina, K.; Sedel, L.; Guillemin, G. Tissue-engineered bone regeneration. *Nat. Biotechnol.* **2000,** *18*, 959-963.
4. Vinatier, C.; Guicheux, J.; Daculsi, G.; Layrolle, P.; Weiss, P. Cartilage and bone tissue engineering using hydrogels. *Biomed. Mater. Eng.* **2006,** *16*, S107-113.
5. Bertolai, R.; Catelani, C.; Aversa, A.; Rossi, A.; Giannini, D.; Bani, D. Bone graft and mesenchimal stem cells: clinical observations and histological analysis. *Clin. Cases Miner. Bone Metab.* **2015,** *12*, 183-187.
6. Burg, K. J.; Porter, S.; Kellam, J. F. Biomaterial developments for bone tissue engineering. *Biomaterials* **2000,** *21*, 2347-2359.
7. Hou, T.; Li, Z.; Luo, F.; Xie, Z.; Wu, X.; Xing, J.; Dong, S.; Xu, J. A composite demineralized bone matrix--self assembling peptide scaffold for enhancing cell and growth factor activity in bone marrow. *Biomaterials* **2014,** *35*, 5689-5699.
8. Finkemeier, C. G. Bone-grafting and bone-graft substitutes. *J. Bone Joint Surg. Am.* **2002,** *84-A*, 454-464.
9. Salama, R. Xenogeneic bone grafting in humans. *Clin. Orthop. Relat. Res.* **1983,** 113-121.
10. Hao, Z.; Song, Z.; Huang, J.; Huang, K.; Panetta, A.; Gu, Z.; Wu, J. The scaffold microenvironment for stem cell based bone tissue engineering. *Biomater. Sci.* **2017,** *5*, 1382-1392.
11. Pina, S.; Oliveira, J. M.; Reis, R. L. Natural-based nanocomposites for bone tissue engineering and regenerative medicine: a review. *Adv. Mater.* **2015,** *27*, 1143-1169.
12. Kriparamanan, R.; Aswath, P.; Zhou, A.; Tang, L.; Nguyen, K. T. Nanotopography: cellular responses to nanostructured materials. *J. Nanosci. Nanotechnol.* **2006,** *6*, 1905-1919.
13. de Oliveira, P. T.; Zalzal, S. F.; Beloti, M. M.; Rosa, A. L.; Nanci, A. Enhancement of in vitro osteogenesis on titanium by chemically produced nanotopography. *J. Biomed. Mater. Res. A.* **2007,** *80*, 554-564.
14. Salmasi, S.; Kalaskar, D. M.; Yoon, W. W.; Blunn, G. W.; Seifalian, A. M. Role of nanotopography in the development of tissue engineered 3D organs and tissues using mesenchymal stem cells. *World J. Stem Cells* **2015,** *7*, 266-280.
15. Lutolf, M. P.; Gilbert, P. M.; Blau, H. M. Designing materials to direct stem-cell fate. *Nature* **2009,** *462*, 433-441.
16. Kaivosoja, E.; Barreto, G.; Levon, K.; Virtanen, S.; Ainola, M.; Konttinen, Y. T. Chemical and physical properties of regenerative medicine materials controlling stem cell fate. *Ann. Med.* **2012,** *44*, 635-650.
17. Stevens, B.; Yang, Y.; Mohandas, A.; Stucker, B.; Nguyen, K. T. A review of materials, fabrication methods, and strategies used to enhance bone regeneration in engineered bone tissues. *J. Biomed. Mater. Res. B. Appl. Biomater.* **2008,** *85*, 573-582.
18. Dvir, T.; Timko, B. P.; Kohane, D. S.; Langer, R. Nanotechnological strategies for engineering complex tissues. *Nat. Nanotechnol.* **2011,** *6*, 13-22.
19. Goldberg, M.; Langer, R.; Jia, X. Nanostructured materials for applications in drug delivery and tissue engineering. *J. Biomater. Sci. Polym. Ed.* **2007,** *18*, 241-268.

20. Ding, Z.; Han, H.; Fan, Z.; Lu, H.; Sang, Y.; Yao, Y.; Cheng, Q.; Lu, Q.; Kaplan, D. L. Nanoscale Silk-Hydroxyapatite Hydrogels for Injectable Bone Biomaterials. *ACS Appl. Mater. Interfaces* **2017,** *9*, 16913-16921.
21. Wang, Y.; Qian, J.; Zhao, N.; Liu, T.; Xu, W.; Suo, A. Novel hydroxyethyl chitosan/cellulose scaffolds with bubble-like porous structure for bone tissue engineering. *Carbohydr. Polym.* **2017,** *167*, 44-51.
22. Lin, Z.; Cao, S.; Chen, X.; Wu, W.; Li, J. Thermoresponsive hydrogels from phosphorylated ABA triblock copolymers: a potential scaffold for bone tissue engineering. *Biomacromolecules* **2013,** *14*, 2206-2214.
23. Thambi, T.; Phan, V. H.; Lee, D. S. Stimuli-Sensitive Injectable Hydrogels Based on Polysaccharides and Their Biomedical Applications. *Macromol. Rapid Commun.* **2016,** *37*, 1881-1896.
24. Radhakrishnan, J.; Subramanian, A.; Krishnan, U. M.; Sethuraman, S. Injectable and 3D Bioprinted Polysaccharide Hydrogels: From Cartilage to Osteochondral Tissue Engineering. *Biomacromolecules* **2017,** *18*, 1-26.
25. Ranga, A.; Lutolf, M. P.; Hilborn, J.; Ossipov, D. A. Hyaluronic Acid Hydrogels Formed in Situ by Transglutaminase-Catalyzed Reaction. *Biomacromolecules* **2016,** *17*, 1553-1560.
26. Malafaya, P. B.; Silva, G. A.; Reis, R. L. Natural-origin polymers as carriers and scaffolds for biomolecules and cell delivery in tissue engineering applications. *Adv. Drug Deliv. Rev.* **2007,** *59*, 207-233.
27. Roseti, L.; Parisi, V.; Petretta, M.; Cavallo, C.; Desando, G.; Bartolotti, I.; Grigolo, B. Scaffolds for Bone Tissue Engineering: State of the art and new perspectives. *Mater. Sci. Eng. C. Mater. Biol. Appl.* **2017,** *78*, 1246-1262.
28. Adler-Abramovich, L.; Gazit, E. The physical properties of supramolecular peptide assemblies: from building block association to technological applications. *Chem. Soc. Rev.* **2014,** *43*, 6881-6893.
29. Adams, D. J.; Topham, P. D. Peptide conjugate hydrogelators. *Soft Matter.* **2010,** *6*, 3707-3721.
30. Tomasini, C.; Castellucci, N. Peptides and peptidomimetics that behave as low molecular weight gelators. *Chem. Soc. Rev.* **2013,** *42*, 156-172.
31. Zhao, F.; Ma, M. L.; Xu, B. Molecular hydrogels of therapeutic agents. *Chem. Soc. Rev.* **2009,** *38*, 883-891.
32. Adams, D. J. Dipeptide and tripeptide conjugates as low-molecular-weight hydrogelators. *Macromol. Biosci.* **2011,** *11*, 160-173.
33. Mata, A.; Geng, Y.; Henrikson, K. J.; Aparicio, C.; Stock, S. R.; Satcher, R. L.; Stupp, S. I. Bone regeneration mediated by biomimetic mineralization of a nanofiber matrix. *Biomaterials* **2010,** *31*, 6004-6012.
34. Hauser, C. A.; Zhang, S. Designer self-assembling peptide nanofiber biological materials. *Chem. Soc. Rev.* **2010,** *39*, 2780-2790.
35. Nune, M.; Kumaraswamy, P.; Krishnan, U. M.; Sethuraman, S. Self-assembling peptide nanofibrous scaffolds for tissue engineering: novel approaches and strategies for effective functional regeneration. *Curr. Protein Pept. Sci.* **2013,** *14*, 70-84.
36. Fichman, G.; Gazit, E. Self-assembly of short peptides to form hydrogels: design of building blocks, physical properties and technological applications. *Acta Biomater.* **2014,** *10*, 1671-1682.
37. Aida, T.; Meijer, E. W.; Stupp, S. I. Functional supramolecular polymers. *Science* **2012,** *335*, 813-817.
38. Raeburn, J.; Zamith Cardoso, A.; Adams, D. J. The importance of the self-assembly process to control mechanical properties of low molecular weight hydrogels. *Chem. Soc. Rev.* **2013,** *42*, 5143-5156.
39. Buerkle, L. E.; Rowan, S. J. Supramolecular gels formed from multi-component low molecular weight species. *Chem. Soc. Rev.* **2012,** *41*, 6089-6102.

40. Safont-Sempere, M. M.; Fernandez, G.; Wurthner, F. Self-sorting phenomena in complex supramolecular systems. *Chem. Rev.* **2011,** *111*, 5784-5814.
41. Raeburn, J.; Adams, D. J. Multicomponent low molecular weight gelators. *Chem. Commun.* **2015,** *51*, 5170-5180.
42. Matson, J. B.; Zha, R. H.; Stupp, S. I. Peptide self-assembly for crafting functional biological materials. *Current Opinion in Solid State and Materials Science* **2011,** *15*, 225-235.
43. Baroli, B. Hydrogels for tissue engineering and delivery of tissue-inducing substances. *J. Pharm. Sci.* **2007,** *96*, 2197-2223.
44. Jayawarna, V.; Richardson, S. M.; Hirst, A. R.; Hodson, N. W.; Saiani, A.; Gough, J. E.; Ulijn, R. V. Introducing chemical functionality in Fmoc-peptide gels for cell culture. *Acta Biomater.* **2009,** *5*, 934-943.
45. Knowles, T. P.; Mezzenga, R. Amyloid Fibrils as Building Blocks for Natural and Artificial Functional Materials. *Adv. Mater.* **2016,** *28*, 6546-6561.
46. Kim, H. D.; Jang, H. L.; Ahn, H. Y.; Lee, H. K.; Park, J.; Lee, E. S.; Lee, E. A.; Jeong, Y. H.; Kim, D. G.; Nam, K. T.; Hwang, N. S. Biomimetic whitlockite inorganic nanoparticles-mediated in situ remodeling and rapid bone regeneration. *Biomaterials* **2017,** *112*, 31-43.
47. Mehrali, M.; Thakur, A.; Pennisi, C. P.; Talebian, S.; Arpanaei, A.; Nikkhah, M.; Dolatshahi-Pirouz, A. Nanoreinforced Hydrogels for Tissue Engineering: Biomaterials that are Compatible with Load-Bearing and Electroactive Tissues. *Adv. Mater.* **2017,** *29*.
48. Meagher, M. J.; Weiss-Bilka, H. E.; Best, M. E.; Boerckel, J. D.; Wagner, D. R.; Roeder, R. K. Acellular hydroxyapatite-collagen scaffolds support angiogenesis and osteogenic gene expression in an ectopic murine model: Effects of hydroxyapatite volume fraction. *J. Biomed. Mater. Res. A.* **2016,** *104*, 2178-2188.
49. Gkioni, K.; Leeuwenburgh, S. C.; Douglas, T. E.; Mikos, A. G.; Jansen, J. A. Mineralization of hydrogels for bone regeneration. *Tissue Eng. Part B Rev.* **2010,** *16*, 577-585.
50. Tavafoghi, M.; Cerruti, M. The role of amino acids in hydroxyapatite mineralization. *J. R. Soc. Interface* **2016,** *13*.
51. Jahromi, M. T.; Yao, G.; Cerruti, M. The importance of amino acid interactions in the crystallization of hydroxyapatite. *J. R. Soc. Interface* **2013,** *10*, 20120906.
52. Flynn, N. E.; Meininger, C. J.; Haynes, T. E.; Wu, G. The metabolic basis of arginine nutrition and pharmacotherapy. *Biomed. Pharmacother.* **2002,** *56*, 427-438.
53. Brasinika, D.; Tsigkou, O.; Tsetsekou, A.; Missirlis, Y. F. Bioinspired synthesis of hydroxyapatite nanocrystals in the presence of collagen and l-arginine: Candidates for bone regeneration. *J. Biomed. Mater. Res. B Appl. Biomater.* **2016,** *104*, 458-469.
54. Gonzalez-McQuire, R.; Chane-Ching, J.-Y.; Vignaud, E.; Lebugle, A.; Mann, S. Synthesis and characterization of amino acid-functionalized hydroxyapatite nanorods. *J. Mater. Chem.* **2004,** *14*, 2277-2281.
55. Palazzo, B.; Walsh, D.; Iafisco, M.; Foresti, E.; Bertinetti, L.; Martra, G.; Bianchi, C. L.; Cappelletti, G.; Roveri, N. Amino acid synergetic effect on structure, morphology and surface properties of biomimetic apatite nanocrystals. *Acta Biomater.* **2009,** *5*, 1241-1252.
56. Mahler, A.; Reches, M.; Rechter, M.; Cohen, S.; Gazit, E. Rigid, Self-Assembled Hydrogel Composed of a Modified Aromatic Dipeptide. *Adv. Mater.* **2006,** *18*, 1365-1370.
57. Hu, Y.; Chen, J.; Fan, T.; Zhang, Y.; Zhao, Y.; Shi, X.; Zhang, Q. Biomimetic mineralized hierarchical hybrid scaffolds based on in situ synthesis of nano-hydroxyapatite/chitosan/chondroitin sulfate/hyaluronic acid for bone tissue engineering. *Colloids Surf. B Biointerfaces* **2017,** *157*, 93-100.
58. Huang, R.; Qi, W.; Feng, L.; Su, R.; He, Z. Self-assembling peptide–polysaccharide hybrid hydrogel as a potential carrier for drug delivery. *Soft Matter.* **2011,** *7*, 6222-6230.

59. Gong, X.; Branford-White, C.; Tao, L.; Li, S.; Quan, J.; Nie, H.; Zhu, L. Preparation and characterization of a novel sodium alginate incorporated self-assembled Fmoc-FF composite hydrogel. *Mater. Sci. Eng. C. Mater. Biol. Appl.* **2016,** *58*, 478-486.
60. Pont, G.; Chen, L.; Spiller, D. G.; Adams, D. J. The effect of polymer additives on the rheological properties of dipeptide hydrogelators. *Soft Matter.* **2012,** *8*, 7797-7802.
61. Kong, J.; Yu, S. Fourier transform infrared spectroscopic analysis of protein secondary structures. *Acta Biochim. Biophys. Sin.* **2007,** *39*, 549-559.
62. Fleming, S.; Frederix, P. W. J. M.; Ramos Sasselli, I.; Hunt, N. T.; Ulijn, R. V.; Tuttle, T. Assessing the Utility of Infrared Spectroscopy as a Structural Diagnostic Tool for β-Sheets in Self-Assembling Aromatic Peptide Amphiphiles. *Langmuir* **2013,** *29*, 9510-9515.
63. Ulijn, R. V.; Smith, A. M. Designing peptide based nanomaterials. *Chem. Soc. Rev.* **2008,** *37*, 664-675.
64. Chakraborty, P.; Bairi, P.; Roy, B.; Nandi, A. K. Improved Mechanical and Electronic Properties of Co-assembled Folic Acid Gel with Aniline and Polyaniline. *ACS Appl. Mater. Interfaces* **2014,** *6*, 3615-3622.
65. Wang, P. Y.; Clements, L. R.; Thissen, H.; Jane, A.; Tsai, W. B.; Voelcker, N. H. Screening mesenchymal stem cell attachment and differentiation on porous silicon gradients. *Adv. Funct. Mater.* **2012,** *22*, 3414-3423.
66. Alakpa, E. V.; Jayawarna, V.; Lampel, A.; Burgess, K. V.; West, C. C.; Bakker, S. C.; Roy, S.; Javid, N.; Fleming, S.; Lamprou, D. A. Tunable Supramolecular Hydrogels for Selection of Lineage-Guiding Metabolites in Stem Cell Cultures. *Chem.* **2016,** *1*, 298-319.
67. Engler, A. J.; Sen, S.; Sweeney, H. L.; Discher, D. E. Matrix elasticity directs stem cell lineage specification. *Cell* **2006,** *126*, 677-689.
68. Yan, C.; Pochan, D. J. Rheological properties of peptide-based hydrogels for biomedical and other applications. *Chem. Soc. Rev.* **2010,** *39*, 3528-3540.
69. Colquhoun, C.; Draper, E. R.; Schweins, R.; Marcello, M.; Vadukul, D.; Serpell, L. C.; Adams, D. J. Controlling the network type in self-assembled dipeptide hydrogels. *Soft Matter.* **2017,** *13*, 1914-1919.
70. Yang, Z.; Gu, H.; Fu, D.; Gao, P.; Lam, J. K.; Xu, B. Enzymatic formation of supramolecular hydrogels. *Adv. Mater.* **2004,** *16*, 1440-1444.
71. Cai, Y.; Liu, Y.; Yan, W.; Hu, Q.; Tao, J.; Zhang, M.; Shi, Z.; Tang, R. Role of hydroxyapatite nanoparticle size in bone cell proliferation. *J. Mater. Chem.* **2007,** *17*, 3780-3787.
72. Kalita, S. J.; Bhardwaj, A.; Bhatt, H. A. Nanocrystalline calcium phosphate ceramics in biomedical engineering. *Mater. Sci. Eng. C.* **2007,** *27*, 441-449.
73. Cai, L.; Guinn, A. S.; Wang, S. Exposed hydroxyapatite particles on the surface of photo-crosslinked nanocomposites for promoting MC3T3 cell proliferation and differentiation. *Acta Biomater.* **2011,** *7*, 2185-2199.
74. Galbraith, C. G.; Sheetz, M. P. Forces on adhesive contacts affect cell function. *Curr. Opin. Cell Biol.* **1998,** *10*, 566-571.